Computational Particle Mechanics (2021) 8:737–749
https://doi.org/10.1007/s40571-020-00367-w

Molecular dynamics performance for coronavirus simulation by C, N, O, and S atoms implementation dreiding force field: drug delivery atomic interaction in contact with metallic Fe, Al, and steel

Aliakbar Karimipour[1] · Ali Amini[2] · Mohammad Nouri[2] · Annunziata D'Orazio[3] · Roozbeh Sabetvand[4] · Maboud Hekmatifar[5] · Azam Marjani[6,7] · Quang-vu Bach[8]

Received: 2 August 2020 / Revised: 13 September 2020 / Accepted: 23 September 2020 / Published online: 17 November 2020

Abstract
Coronavirus causes some illnesses to include cold, COVID-19, MERS, and SARS. This virus can be transmitted through contact with different atomic matrix between humans. So, this atomic is essential in medical cases. In this work, we describe the atomic manner of this virus in contact with various metallic matrix such as Fe, Al, and steel with equilibrium molecular dynamic method. For this purpose, we reported physical properties such as temperature, total energy, distance and angle of structures, mutual energy, and volume variation of coronavirus. In this approach, coronavirus is precisely simulated by O, C, S, and N atoms and they are implemented dreiding force field. Our simulation shows that virus interaction with steel matrix causes the maximum removing of the virus from the surfaces. After 1 ns, the atomic distance between these two structures increases from 45 to 75 Å. Furthermore, the volume of coronavirus 14.62% increases after interaction with steel matrix. This atomic manner shows that coronavirus removes and destroyed with steel surface, and this metallic structure can be a promising material for use in medical applications.

Keywords Coronavirus · Molecular dynamic simulation · Atomic interaction · Metallic matrix

1 Introduction

Coronaviruses are a group of connected RNA viruses that origin illnesses in birds and mammals. In humans, these viruses cause some problem in respiratory system infections that can range from mild to lethal. Mild diseases contain some cases of cold and fatal varieties can cause diseases such as MERS, COVID-19, and SARS. There are any vaccines or antiviral drugs to stop or remedy human coronaviruses infections yet. Coronaviruses constitute the subfamily Orthocoronavirinae, in the family Coronaviridae, order Nidovirales, and realm Riboviria [1, 2]. Historically, coronavirus was recognized in the 1930s for the first time [3]. This virus depicted in Fig. 1.

Researchers reported a new respiratory infection of chickens in North Dakota in 1931. The infection of chicks was distinguished by listlessness and gasping. The death rate of the chickens was up to 90% [5, 6]. Transmissible gastroen-

✉ Azam Marjani
azam.marjani@tdtu.edu.vn

✉ Quang-vu Bach
bachquangvu@tdtu.edu.vn

1 Institute of Research and Development, Duy Tan University, Da Nang 550000, Vietnam

2 Department of Mechanical Engineering, Najaf Abad University, Esfahan, Iran

3 Dipartimento di Ingegneria Astronautica, Elettrica ed Energetica, Sapienza Università di Roma, Via Eudossiana 18, 00184 Roma, Italy

4 Department of Energy Engineering and Physics, Faculty of Condensed Matter Physics, Amirkabir University of Technology, Tehran, Iran

5 Department of Mechanical Engineering, Khomeini Shahr University, Esfahan, Iran

6 Department for Management of Science and Technology Development, Ton Duc Thang University, Ho Chi Minh City, Vietnam

7 Faculty of Applied Sciences, Ton Duc Thang University, Ho Chi Minh City, Vietnam

8 Sustainable Management of Natural Resources and Environment Research Group, Faculty of Environment and Labour Safety, Ton Duc Thang University, Ho Chi Minh City, Vietnam

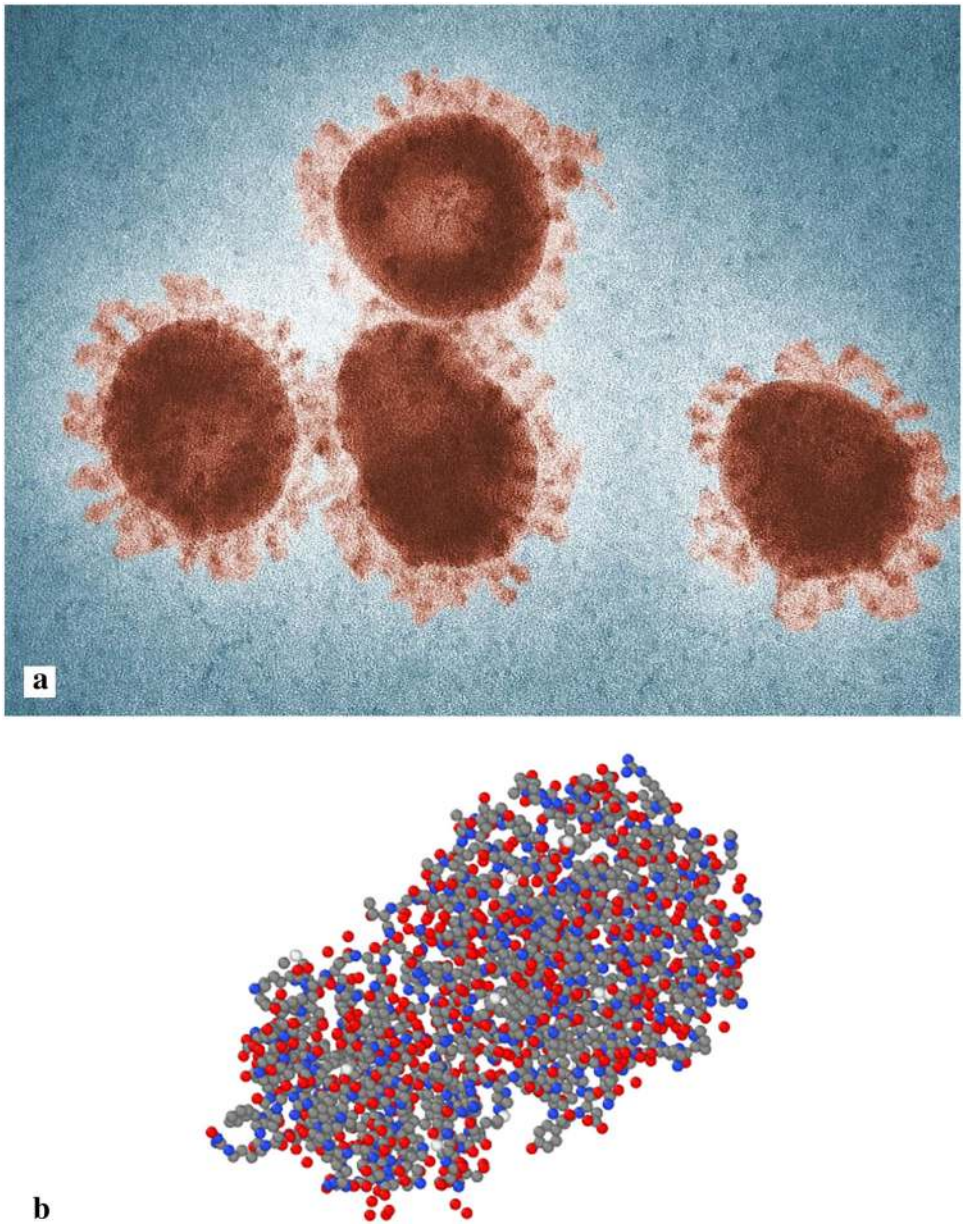

Fig. 1 **a** The common structure of coronavirus recognized by doing some experiment researches. **b** All-atom depiction of the coronavirus simulated using the MD approach [4]

teritis and mouse hepatitis virus were detected in the 1940s [7]. Chemically, these structures are enveloped viruses with a nucleocapsid of helical symmetry and a single-stranded RNA genome which located in an icosahedral protein shell [8]. This atomic structure is one of the biggest thorugh RNA viruses. The genome size of coronaviruses ranges from about 26 to 32 kilobases [4, 9]. Today, numerous researches have been done on the characteristics of this virus. Masters addressed the present state of comprehension of coronavirus genome packaging, which has mainly been studied in 2 prototype species, transmissible gastroenteritis virus, and mouse hepatitis virus [10]. Lu er al. [11] phylogenetic analysis shows that bats, an animal sold at the seafood market in Wuhan, might be the original host of this virus in human.

Furthermore, the structural analysis of this research group suggested that coronavirus might be able to bind to the angiotensin-converting enzyme 2 receptors in humans. Then researchers introduce evolutionary features of the coronaviruses and successfully predicted new coronavirus outbreak by pointing out that novel pathogenic variants will readily appear from very various severe acute respiratory syndrome-related coronaviruses of the bat origin through their close coexistence and high genetic recombination potential [12]. Contrary to many studies, it is not known how the coronavirus interacts with the human environment, such as metallic structures. In this work, we study the coronavirus atomic interaction with metallic surfaces with MD [13–18]. Investigations are provided for the coronavirus and metallic

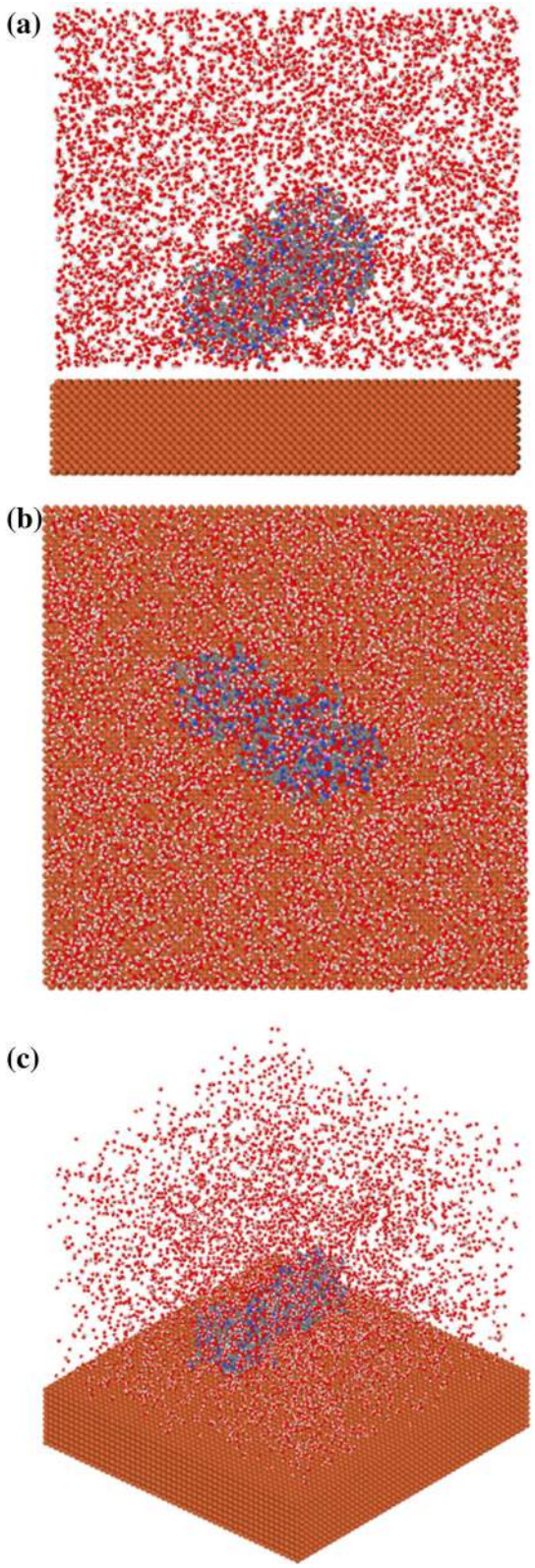

Fig. 2 Schematic of coronavirus/H_2O molecules mixture and metallic matrix (Fe structure) which prepared via Packmol box at **a** front, **b** top, and **c** perspective views

Table 1 The ε and σ constants for LJ interaction in coronavirus MD simulation [52]

	ε (kcal/mol)	σ (A)
Carbon	0.3050	4.180
Nitrogen	0.4150	3.995
Oxygen	0.4150	3.710
Sulfur	0.3050	4.240

Table 2 The r_0 and θ_0 rates of coronavirus structure in our MD simulations [52]

Bond/angle	r_0 (Å)	θ_0 (°)
CC	1.530	–
NC	1.462	–
OC	1.420	–
SC	1.800	–
ON	1.352	–
CCC	–	109.471
CNC	–	106.700
CSC	–	92.100
NCC	–	109.471
NCN	–	109.471
OCC	–	109.471
OCO	–	109.471
SCC	–	109.471
NOC	–	104.510
ONC	–	106.700

matrix (Fe, Al, and steel structures) interactions at various temperatures (300–350 K) in this paper. For this purpose temperature, potential energy, center of mass (COM) distance, COM angles, mutual energy, and volume of simulated structures are reported.

2 Numerical method

In this computational study, we used MD simulation to calculate the atomic behavior of coronavirus in contact with metallic surfaces such as Fe, Al, and steel. Molecular dynamics method is a way for calculating the dynamical evolution of atoms and molecules. In MD method, atoms and molecules are allowed to atomic interaction and give a view of the position and velocity changes of the total system. In the research, all MD simulations were done via LAMMPS [19–22]. This computational package designing began in the 1990s by Sandia and LLNL laboratories. To use this package to calculate the atomic behavior of coronavirus, this atomic structure, H_2O molecules, and metallic matrix were simulated. For this, coronavirus structure was situated in the middle region of MD simulation package, while the other regions of MD simulation box was filled by H_2O structure. This initial atomic positions prepared via Packmol package [23]. Figure 2 displays the MD simulation package at the front, top,

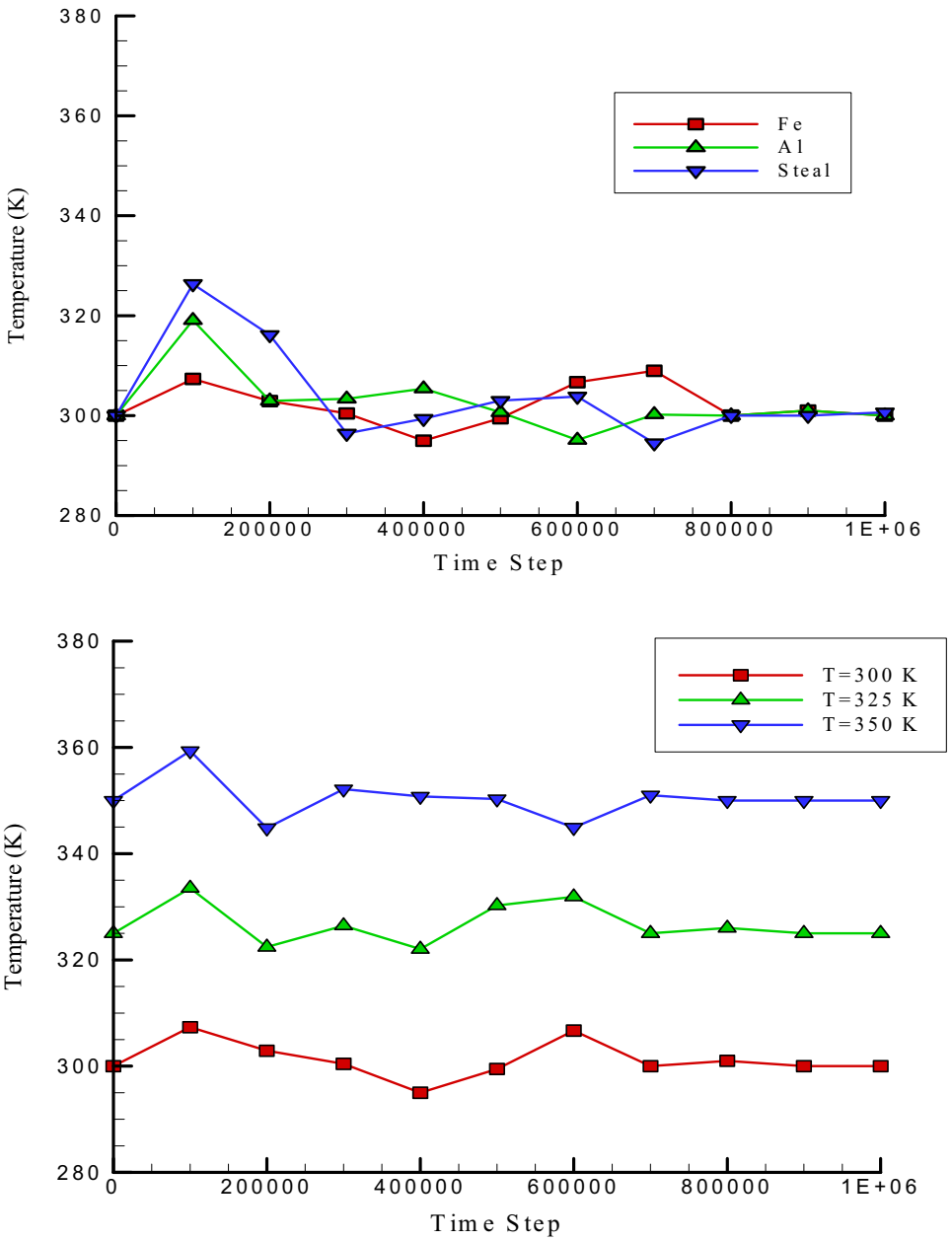

Fig. 3 Temperature variation of simulated structures at **a** various initial temperatures and **b** various metallic matrix as a function of MD simulation time steps

and perspective views, which were depicted by open visualization tool (OVITO) [24]. Particle base methods such as MD, LBM [25–36], or nanoparticles dispersed in the base fluid can be estimated as the various approaches of investigation through such that problem [37–51].

In this molecular dynamics simulations, periodic boundary conditions were used in x, y, and z directions. For preparing the initial temperature of simulated structures, the thermostat was used in the MD simulation box to equilibrate this physical parameter at 300 K, 325 K and 350 K with 1 femtosecond time step. After 1,000,000 MD simulation time steps, at the selected temperature, the simulated atomic structures were equilibrated; then, micro-canonical ensemble (NVE) was implemented to describe the virus and metallic surfaces atomic interaction. To simulate the coronavirus atomic structure, we use the dreiding force field [52]. This interatomic force field is the appropriate choice to biological mixtures MD simulation. In dreiding force field, the potential of various atoms was described as a non-bonded and bonded forces. Non-bond force between particles in dreiding force field described by the Lennard–Jones (LJ) formalism. This formalism is a mathematically simple relation about the interatomic force between a pair of particles. This simple

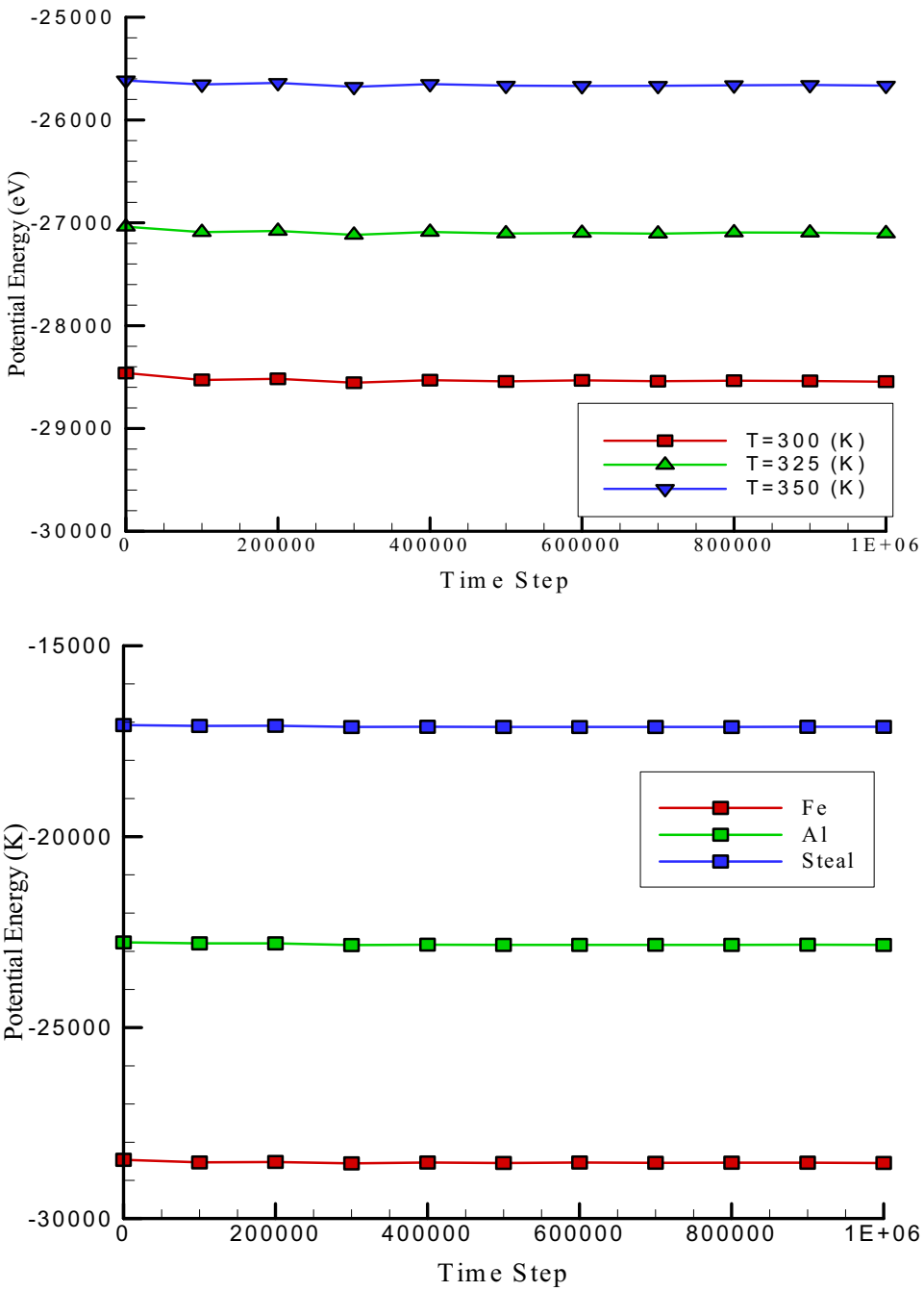

Fig. 4 Potential energy variation of simulated structures at **a** various initial temperatures and **b** various metallic matrix

relation was stated by Lennard Jones [53] for the first time. This simple atomic interaction stated as Eq. (1):

$$U(r) = 4\varepsilon\left[\left(\frac{\sigma}{r_{ij}}\right)^{12} - \left(\frac{\sigma}{r_{ij}}\right)^{6}\right] \quad r \ll r_c \tag{1}$$

In Eq. (1), σ is the distance at which the function is zero; ε is the depth of the potential well, and r_{ij} is the distance between the two atoms. In MD simulations, both σ and ε constants related to the kind of the particles in the MD simulation package. The length scale parameter, cutoff radius, and energy for various atoms in coronavirus simulation are classified in Table 1 [52].

The bonded forces consist of bond angle bend, bond strength, and dihedral angle torsion terms. The bond and

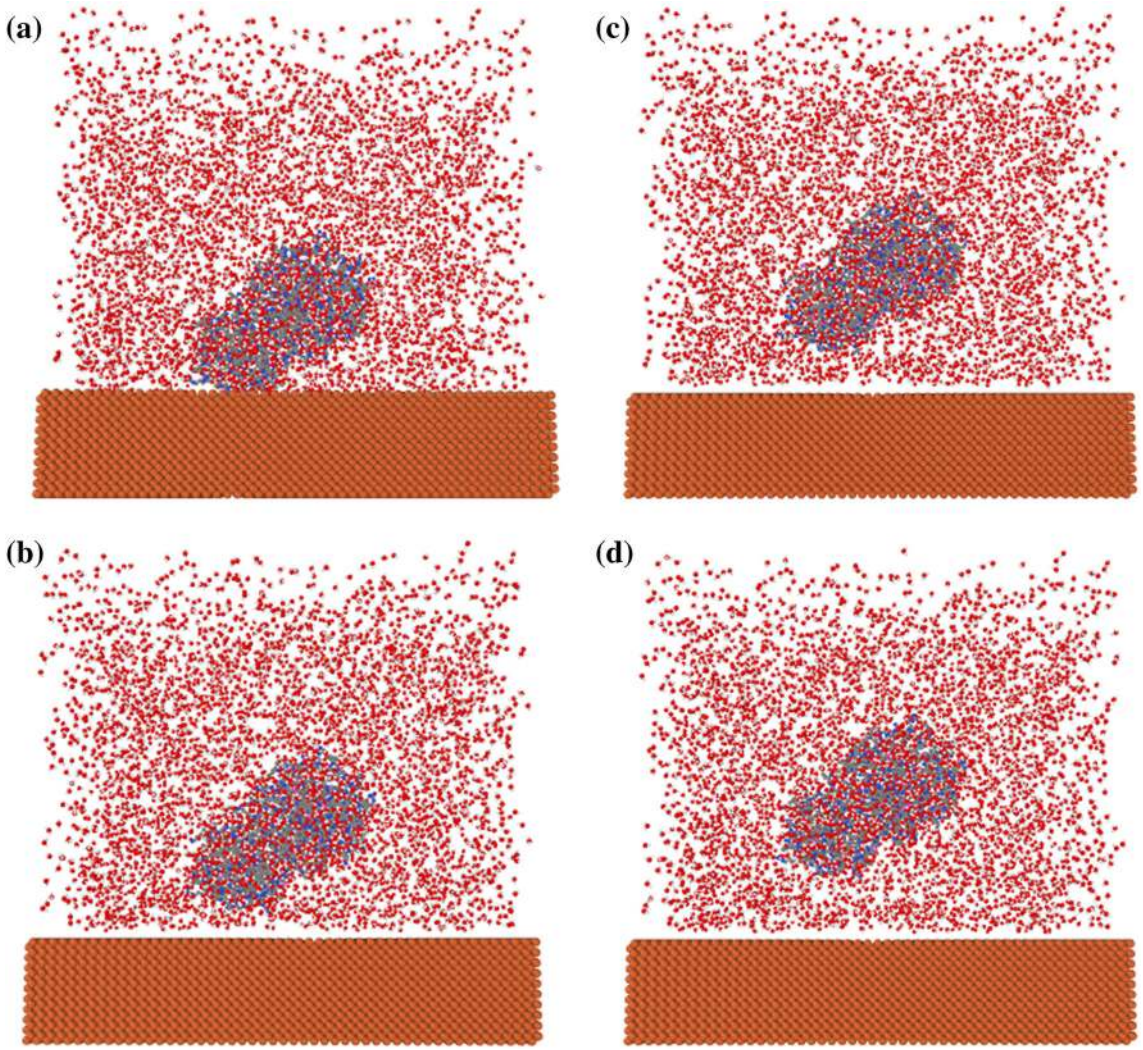

Fig. 5 Time evolution of coronavirus and metallic matrix with COM distance for **a** 0.5 ns, **b** 1 ns, **c** 1.5 ns, and **d** 2 ns

angle strength stretch in dreiding force field are calculated by harmonic oscillator equations as (2) and (3) formulas:

$$E_r = \frac{1}{2}k_r(r - r_0) \tag{2}$$

$$E_\theta = \frac{1}{2}k_\theta(\theta - \theta_0) \tag{3}$$

In these formulas, K_θ and K_r are harmonic oscillator constants. θ_0 is the equilibrium value of angles, and r_0 is the atomic bond length. K_θ and K_r constants in coronavirus MD study were selected at 100 (kcal/mol)/degree^2 and 300 (kcal/mol)/A^2, respectively. Furthermore, the r_0 and θ_0 constants in our MD simulations are classified in Table 2 [52]. Dihedral term in atomic interaction described with Eq. (4) and its coefficients are chosen from a dreiding force field [52]:

$$E = K(1 + d\cos(n\varphi) \tag{4}$$

In Eq. (4), K is an oscillator constant with + 1 or − 1 rates and the integer number is n [52].

Today, various atomic models such as SPC, TIP4P, and TIP3P are used to molecular dynamics simulation of water atomic structure. In SPC model, three sites were used for the electrostatic interactions and the positive charges on the hydrogen atoms were neutralized by a negative charge. The interaction between H_2O molecules were simulated using a LJ potential. These interaction parameters for atomic water structure are reported in [54, 55]:

O weight = 15.9994 u
H weight = 1.008 u
O atomic charge = − 0.820
H atomic charge = 0.410
ε constant for O–O interaction = 0.1553 kcal/mol
σ constant for O–O interaction = 3.166 Å
ε and σ constants for O–H and H–H interactions = 0.0

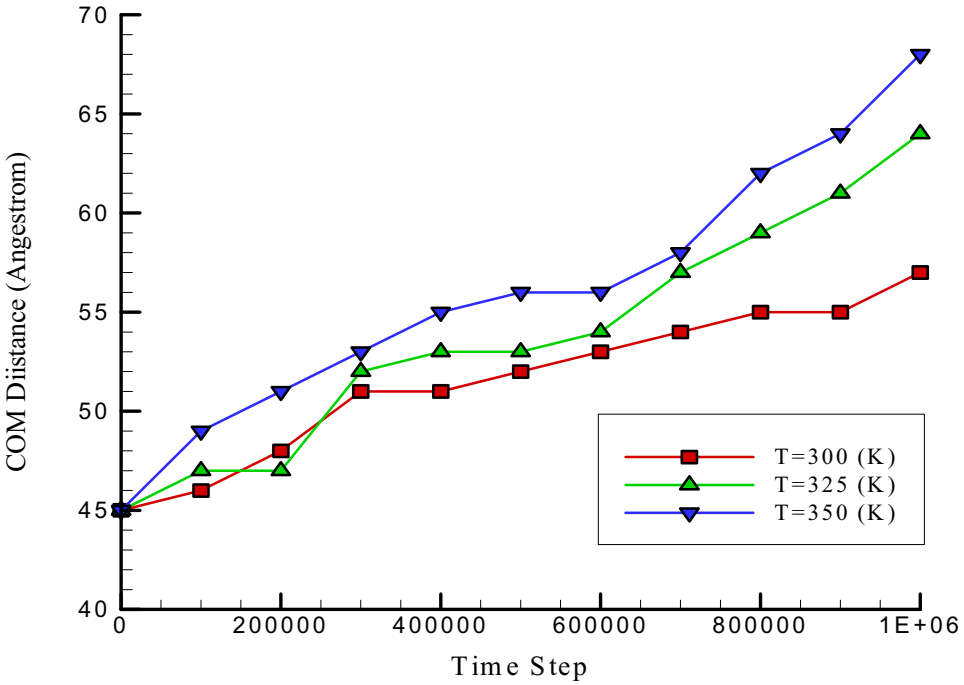

Fig. 6 COM distance variation of coronavirus and Fe matrix with MD simulation time steps and sample temperature

Table 3 COM distance of coronavirus and metallic matrix

Temperature (K)	Fe atomic distance (Å)	Al atomic distance (Å)	Steel atomic distance (Å)
300	57	59	61
325	64	67	70
350	68	71	75

Table 4 COM angle of coronavirus with a metallic matrix

Temperature (K)	Fe atomic angle	Al atomic angle	Steel atomic angle
300	92	89	93
325	95	88	91
350	88	91	92

r_0 constant for OH bond = 1.0 Å
θ_0 constant for HOH angle = 109.47∘

Furthermore, metallic structures in our MD simulations described by inserted atom model (EAM) force field [56]. EAM force field is represented by Eq. (5):

$$E_i = F_\alpha\left(\sum_{i\neq j}\rho_\beta\left(r_{ij}\right)\right) + \frac{1}{2}\sum_{i\neq j}\phi_{\alpha\beta}\left(r_{ij}\right) \tag{5}$$

In this equation, r_{ij} is the distance between i and j particles, $\phi_{\alpha\beta}$ is a pair-wise potential function, $\rho_{\alpha\beta}$ is the contribution to the electron density from particle j of type β at the location of particle i, and F_α is an embedding function that stats the energy required to place particle i of type α into the electron distribution. After atomic modeling and force field implementing, the atomic manner of coronavirus in the vicinity of metallic matrix estimated. For computations of these atomic evolutions, Newton's second law [13, 14],

$$F_i = \sum_{i\neq j} F_{ij} = m_i\frac{\mathrm{d}^2 r_i}{\mathrm{d}t^2} = m_i\frac{\mathrm{d}v_i}{\mathrm{d}t} \tag{6}$$

Which leads to [13, 14]:

$$F_i = -\sum \mathrm{grad}\, V_{ij}\left(r_{ij}\right) \tag{7}$$

Temperature from the Gaussian distribution [13, 14]:

$$\frac{3}{2}k_\mathrm{B}T = \frac{1}{N_\mathrm{atom}}\sum_{i=1}^{N}\frac{1}{2}mv_i^2 \tag{8}$$

Association of Eq. (6) is provided by velocity Verlet algorithm.

$$v(t+\delta t) = v(t) + a(t)\delta t \tag{9}$$

$$r(t+\delta t) = r(t) + v(t)\delta t \tag{10}$$

In these Eqs. (9) and (10), $r(t+\delta t)$, $v(t+\delta t)$ is the final coordination and velocity of particles and $v(t)$ and $r(t)$ are

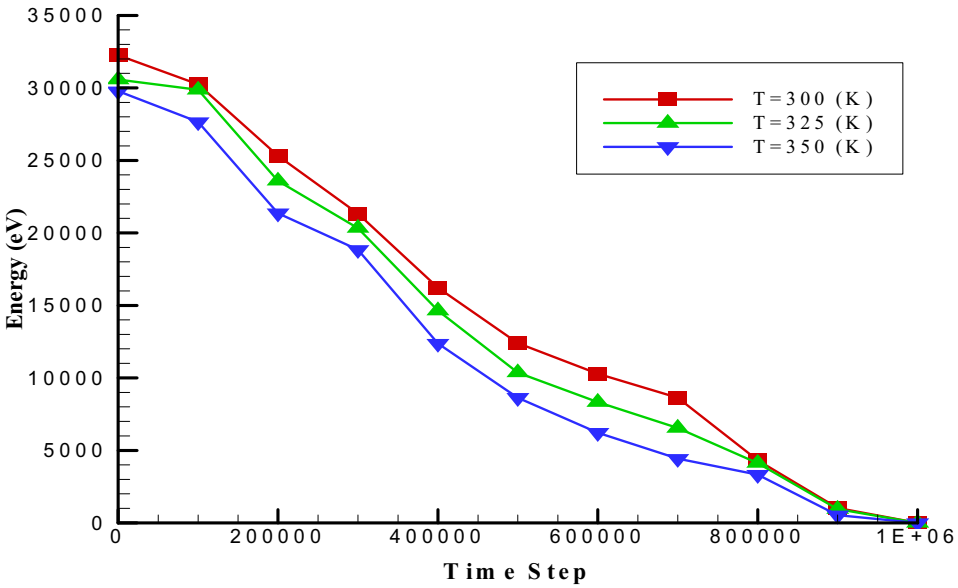

Fig. 7 Common energy variation of coronavirus and Fe matrix with MD simulation time steps and temperature

Table 5 Common energy variation of coronavirus and metallic matrix

Temperature (K)	Fe matrix (eV)	Al matrix (eV)	Steel matrix (eV)
300	32,261	28,759	25,222
325	30,569	27,569	22,359
350	29,777	26,335	19,965

the rate of these physical parameters at $t = 0$. Finally, we can say that MD simulations of this work in 2 steps [57–59]:

Step A Coronavirus and metallic matrix were simulated at 300, 325, and 350 K with 1 fs time step.
Step B In the second step of our molecular dynamics simulation, the atomic interaction between the virus and metallic matrix was carried out for 1,000,000 MD simulation time steps.

3 Results

3.1 Equilibration process of atomic structures

In the first step of this molecular dynamics simulations, the atomic structure of the coronavirus and metal surfaces was studied. Figure 3 shows the atomic arrangement of structures in our simulation box [52]. Numerically, structures atomic stability are described by reporting of temperature and potential energy of them at 300 K, 325 K, and 350 K. Temperature variation of various structures is depicted in Fig. 3. From this figure, we can say that all structures thermally equilibrated after 1,000,000 MD simulation time steps passing. Figure 4 displays the potential energy. We can say that the simulated structures potential energy converged after 1,000,000-time steps. This result shows that dreiding force field has good ability in bio structures simulations. Numerically, the potential energy of the coronavirus structure with Fe matrix decreases from − 28,545 to − 25,665 eV by temperature increasing from 300 to 350 K. This atomic manner shows the kinetic energy increasing in simulated structures which this parameter increasing cause the mean distance of atomic structure rises. It can be said that simulated structures with Fe matrix have better stability rather than Al and Steel matrix and by temperature increasing this stability decreases (see Fig. 4). Furthermore, coronavirus atomic stability reaches to minimum rate in the presence of steel matrix, while this atomic behavior of the coronavirus makes the steel matrix work best in medical applications.

3.2 Dynamical evolution

The COM of the atomic structures is one of the geometrical. The interatomic force between the coronavirus and metallic surface is repulsive (Fig. 5). Numerically, the distance of coronavirus and Fe atoms varies from 45 to 57 Å at 300 K. This physical parameter increases by temperature increasing from 300 to 350 K (see Fig. 6 and Table 3). As reported in Table 3, steel and aluminum matrix interaction with coronavirus shows a similar manner and steel matrix shows maximum atomic distance from the coronavirus after 1,000,000-time steps. Furthermore, as seen in Table 4, the angle of the coronavirus with all matrix surface fluctuates with temperature increasing. This geometrical parameter has 92°, 95°, and 88° at 300 K, 325 K and 350 K for Fe matrix

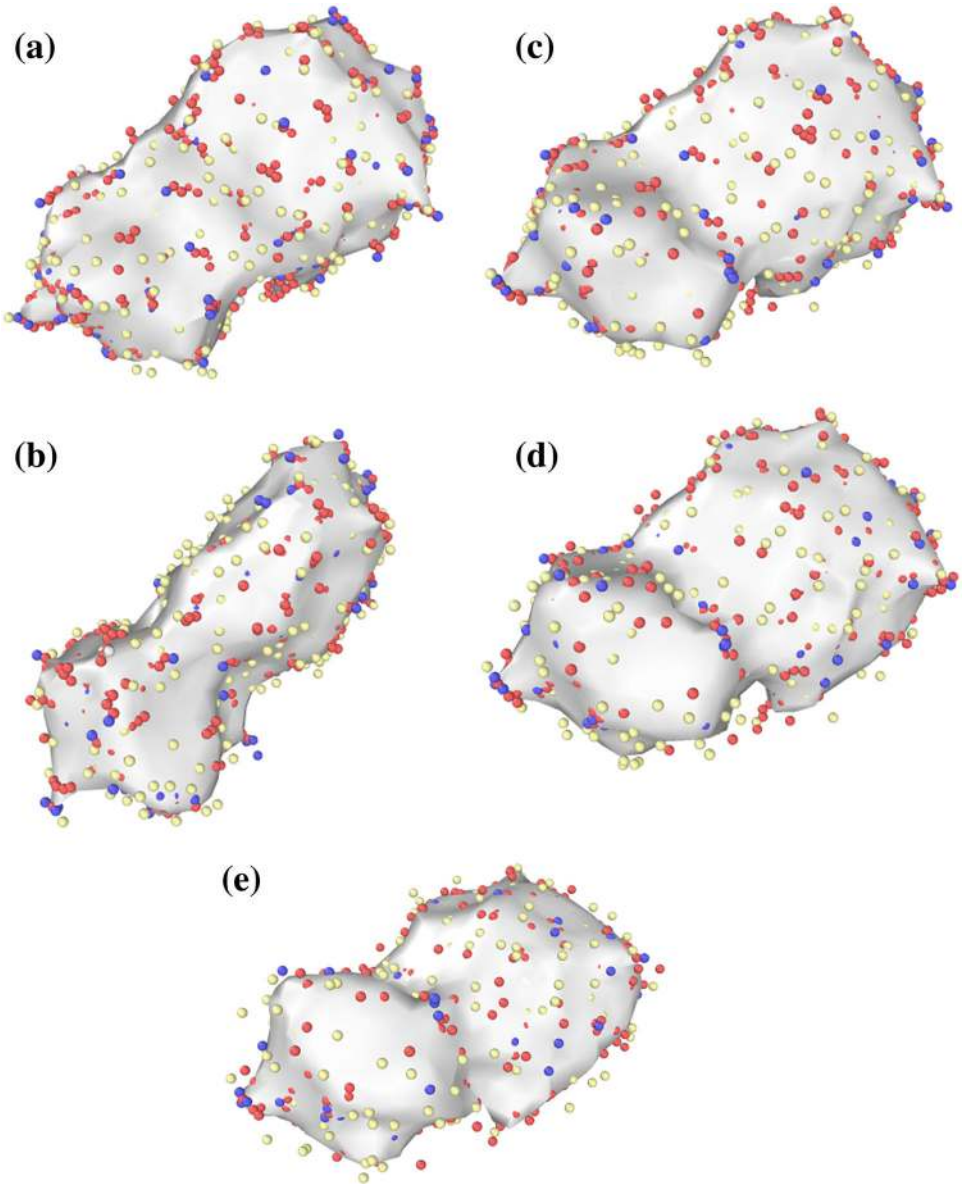

Fig. 8 Variation of coronavirus volume with time steps: **a** n = 0, **b** $n = 250{,}000$, $n = 500{,}000$, $n = 750{,}000$, and $n = 1{,}000{,}000$

surface, respectively. So by increasing temperature, the angle of the coronavirus does not follow a logical relation.

Mutual energy of two groups of simulated structures describes their atomic interaction in MD simulations. In this step of our calculations, we report the mutual energy of coronavirus and metallic matrix. Figure 7 shows that the mutual energy between the coronavirus and Fe matrix varies from 32,261/30,569/29,777 to 0 eV by temperature increasing. Zero rates of mutual energy rate show that the coronavirus structure and Fe matrix distance are bigger than the cutoff radius of them at 350 K and these structures departed from each other after 1,000,000-time steps. Coronavirus with Al and steel matrix interacts with a similar manner, and mutual energy of these structures decreases by MD simulation time steps passing (Table 5). Between metallic matrix, steel one has minimum mutual interaction with the coronavirus. That implies the antivirus property of this structure which nominated this metal to antibacterial applications.

Larger simulation time steps, volume of virus structure rises in the presence of steel atoms and so, the atomic distance increases, too (see Fig. 8). More the distance of atoms in the coronavirus structure, the stability of the virus decreases. From Fig. 9 by the time evolution from 0 to 1,000,000-time steps, the volume of coronaviruses increases from 179,091 to 205,283 $Å^3$. Coronavirus volume does not change drastically by simulation time evolution in the presence of Fe and Al

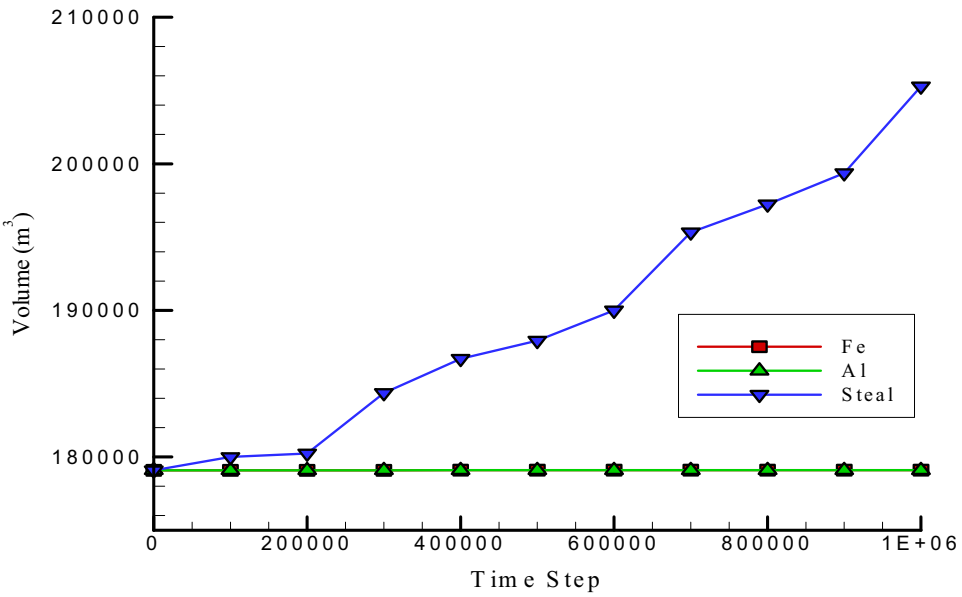

Fig. 9 Coronavirus volume variation with metallic matrix and MD simulation time steps

Table 6 Coronavirus volume variation with metallic matrix at $T = 300$ K

Matrix type	Volume(Å^3)
Fe	179,095
Al	179,098
Steel	205,283

Table 7 Coronavirus volume variation with metallic matrix and molecular dynamics simulation temperature

Temperature (K)	Fe matrix (Å^3)	Al matrix (Å^3)	Steel matrix (Å^3)
300	179,095	179,098	205,283
325	179,123	179,269	223,698
350	179,359	181,433	253,244

matrix (Table 6). Volume of the virus varies from 179,091 to 179,095/179,098 Å^3 for Fe/Al matrix, respectively. This atomic behavior indicates that the use of steel in medical applications can have an important role in the elimination of coronavirus.

Furthermore, with temperature increasing from 300 to 350 K, the final volume of coronavirus varies from 205,283 to 253,244 Å^3 in the presence of steel matrix (Table 7). Figure 10 shows the volume variation of the coronavirus structure in the presence of various metallic matrix. From these results, we can say that coronavirus atomic stability do not reduce in the presence of Fe and Al matrix.

4 Conclusion

The present study investigates the atomic interaction between the coronavirus and metallic matrix such as Fe, Al, and steel with MD simulations. In our calculations, the coronavirus is shown by S,O, N, and C atoms. Result of simulations shows that steel matrix has good properties to prevent coronavirus transmission, which can be used for medical purposes. Generally, the results are as following:

- Dreiding force field is the appropriate interatomic potential for MD simulation of coronavirus. Numerically, the total energy of our simulated structures converged to − 28,545 eV, − 22,835 eV, and − 17,124 eV after 1 ns at 300 K in the presence of Fe, Al, and steel matrix.
- Center of the mass distance of coronavirus and metallic structures increases by the passage of MD simulations time from 45 to 75 Å where the largest rate of this physical parameter occurs for steel matrix.
- Generally, by increasing the simulation temperature, the atomic repulsion between the metallic matrix and coronavirus rises.
- By increasing the temperature of simulated structures, the angle of the coronavirus does not follow a logical relation
- The mutual energy of coronavirus and metallic structures varies from 19,965 to 32,261 eV after 1 ns. The highest rate of this physical parameter calculated for the Fe matrix, which describes maximum interaction between the coronavirus and these metallic structures in our MD simulations.

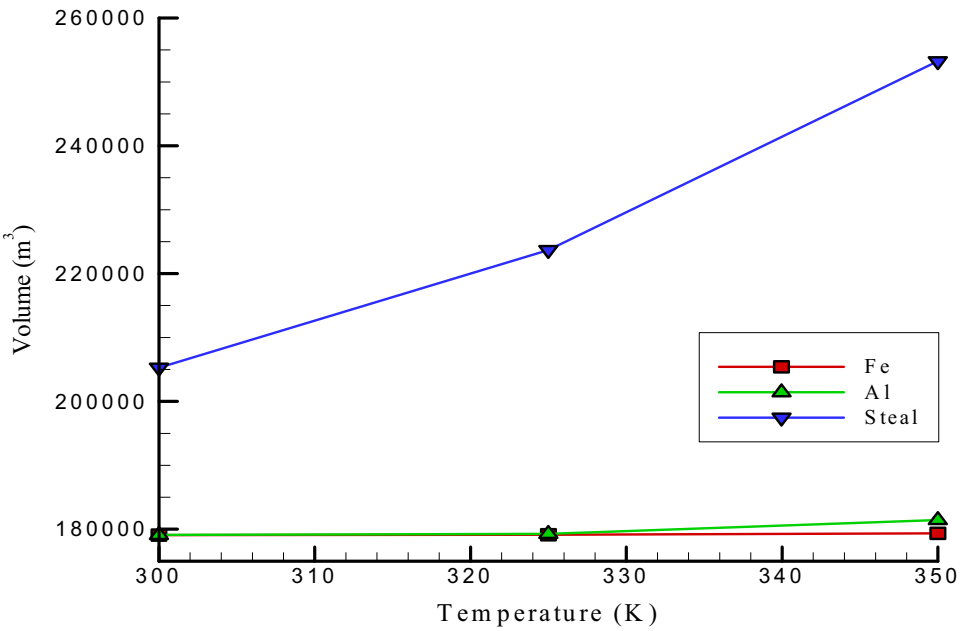

Fig. 10 Time evolution of coronavirus volume in vicinity of metallic matrix with MD simulation temperature

The volume of the coronavirus increases by MD simulation time passing in the presence of steel matrix. Numerically, coronavirus volume increases from 179,091 to 253,244 after atomic interaction with steel matrix.

Compliance with ethical standards

Conflict of interest There is no conflict of interest.

References

1. de Groot RJ, Baker SC, Baric R, Enjuanes L, Gorbalenya AE, Holmes KV, Perlman S, Poon L, Rottier PJ, Talbot PJ, Woo PC, Ziebuhr J (2011) Family Coronaviridae. In: King AM, Lefkowitz E, Adams MJ, Carstens EB, International Committee on Taxonomy of Viruses, International Union of Microbiological Societies. Virology Division (eds) Ninth report of the international committee on taxonomy of viruses. Elsevier, Oxford, pp 806–828
2. Cherry J, Demmler-Harrison GJ, Kaplan SL, Steinbach WJ, Hotez PJ (2017) Feigin and Cherry's textbook of pediatric infectious diseases. Elsevier Health Sciences, Philadelphia, p PT6615. ISBN 978-0-323-39281-5
3. Estola T (1970) Coronaviruses, a new group of animal RNA viruses. Avian Dis 14(2):330–336
4. Almeida JD, Berry DM, Cunningham CH, Hamre D, Hofstad MS, Mallucci L, McIntosh K, Tyrrell DA (1968) Virology: coronaviruses. Nature 220(5168):650
5. Fabricant J (1998) The early history of infectious bronchitis. Avian Dis 42(4):648–650
6. Decaro N (2011) Gammacoronavirus. In: Tidona C, Darai G (eds) Gammacoronavirus‡: coronaviridae. The Springer Index of Viruses. Springer, Berlin, pp 403–413
7. McIntosh K (1974) Coronaviruses: a comparative review. In: Arber W, Haas R, Henle W, Hofschneider PH, Jerne NK, Koldovský P, Koprowski H, Maaløe O, Rott R (eds) Current topics in microbiology and immunology/Ergebnisse der Mikrobiologie und Immunitätsforschung. Springer, Berlin, p 87
8. Fan Y, Zhao K, Shi ZL, Zhou P (2019) Bat coronaviruses in China. Viruses 11(3):210
9. Woo PC, Huang Y, Lau SK, Yuen KY (2010) Coronavirus genomics and bioinformatics analysis. Viruses 2(8):1804–1820. https://doi.org/10.3390/v2081803
10. Masters PS (2019) Coronavirus genomic RNA packaging. Virology 537:198–207
11. Lu R, Zhao X, Li J (2020) Genomic characterisation and epidemiology of 2019 novel coronavirus: implications for virus origins and receptor binding. The Lancet 395(10224):565–574
12. Cui J, Li F, Shi Z-L (2018) Origin and evolution of pathogenic coronaviruses. Nat Rev Microbiol 17:181–192
13. Alder BJ, Wainwright TE (1959) Studies in molecular dynamics. I. General method. J Chem Phys 31(2):459
14. Rahman A (1964) Correlations in the motion of atoms in liquid argon. Phys Rev 136(2A):A405–A411
15. Sabetvand R, Ghazi ME, Izadifard M (2020) Studying temperature effects on electronic and optical properties of cubic $CH_3NH_3SnI_3$ perovskite. J Comput Electron 19:70–79
16. Ghanbari A, Warchomicka F, Sommitsch C, Zamanian A (2019) Investigation of the oxidation mechanism of dopamine functionalization in an AZ31 magnesium alloy for biomedical applications. Coatings 9(9):584
17. Jolfaei NA, Jolfaei NA, Hekmatifar M, Piranfar A, Toghraie D, Sabetvand R, Rostami S (2019) Investigation of thermal properties of DNA structure with precise atomic arrangement via equilibrium and non-equilibrium molecular dynamics approaches. Comput Methods Programs Biomed 185:105169
18. Ashkezari AZ, Jolfaei NA, Jolfaei NA, Hekmatifar M, Toghraie D, Sabetvand R, Rostami S (2019) Calculation of the thermal conductivity of Human Serum Albumin (HSA) with equilibrium/non-equilibrium molecular dynamics approaches. Comput Methods Programs Biomed 188:105256
19. Brown WM, Wang P, Plimpton SJ, Tharrington AN (2011) Implementing molecular dynamics on hybrid high performance computers–short range forces. Comput Phys Commun 182:898–911
20. Brown WM, Kohlmeyer A, Plimpton SJ, Tharrington AN (2012) Implementing molecular dynamics on hybrid high performance

computers—particle–particle particle-mesh. Comput Phys Commun 183(3):449–459
21. Plimpton S (1995) Fast parallel algorithms for short-range molecular dynamics. J Comput Phys 117(1):1–19
22. Mukherjee R, Crozier PS, Plimpton SJ, Anderson KS (2008) Substructured molecular dynamics using multibody dynamics algorithms. Int J Non-Linear Mech 43(10):1040–1055
23. Martinez L, Andrade R, Birgin EG, Martínez JM (2009) PACKMOL: a package for building initial configurations for molecular dynamics simulations. J Comput Chem 30(13):2157–2164
24. Stukowski A (2009) Visualization and analysis of atomistic simulation data with OVITO–the open visualization tool. Model Simul Mater Sci Eng 18(1):015012
25. Akbari OA, Safaei MR, Goodarzi M, Akbar NS, Zarringhalam M, Shabani GAS, Dahari M (2016) A modified two-phase mixture model of nanofluid flow and heat transfer in a 3-D curved microtube. Adv Powder Technol 27:2175–2185
26. Akbari OA, Toghraie D, Karimipour A, Safaei MR, Goodarzi M, Alipour H, Dahari M (2016) Investigation of rib's height effect on heat transfer and flow parameters of laminar water-Al_2O_3 nanofluid in a rib-microchannel. Appl Math Comput 290:135–153
27. Bahiraei M, Jamshidmofid M, Goodarzi M (2019) Efficacy of hybrid nanofluid in a new microchannel heat sink equipped with both secondary channels and ribs. J Mol Liq 273:88–98
28. Goodarzi M, Safaei MR, Karimipour A, Hooman K, Dahari M, Kazi SN, Sadeghinezhad E (2014) Comparison of the finite volume and lattice Boltzmann methods for solving natural convection heat transfer problems inside cavities and enclosures. In: Abstract and applied analysis, Hindawi
29. Arani AAA, Akbari OA, Safaei MR, Marzban A, Airashed A, Ahmadi GR, Nguyen TK (2017) Heat transfer improvement of water/single-wall carbon nanotubes (SWCNT) nanofluid in a novel design of a truncated double-layered microchannel heat sink. Int J Heat Mass Transf 113:780–795
30. Behnampour A, Akbari OA, Safaei MR, Ghavami M, Marzban A, Shabani GAS, Zarringhalam M, Mashayekhi R (2017) Analysis of heat transfer and nanofluid fluid flow in microchannels with trapezoidal, rectangular and triangular shaped ribs. Phys E Low Dimens Syst Nanostruct 91:15–31
31. Heydari A, Akbari OA, Safaei MR, Derakhshani M, Alrashed A, Mashayekhi R, Shabani GAS, Zarringhalam M, Nguyen TK (2018) The effect of attack angle of triangular ribs on heat transfer of nanofluids in a microchannel. J Therm Anal Calorim 131:2893–2912
32. Khodabandeh E, Safaei MR, Akbari S, Akbari OA, Alrashed A (2018) Application of nanofluid to improve the thermal performance of horizontal spiral coil utilized in solar ponds: geometric study. Renew Energy 122:1–16
33. Maleki H, Safaei MR, Alrashed A, Kasaeian A (2019) Flow and heat transfer in non-Newtonian nanofluids over porous surfaces. J Therm Anal Calorim 135:1655–1666
34. Maleki H, Safaei MR, Togun H, Dahari M (2019) Heat transfer and fluid flow of pseudo-plastic nanofluid over a moving permeable plate with viscous dissipation and heat absorption/generation. J Therm Anal Calorim 135:1643–1654
35. Moradikazerouni A, Hajizadeh A, Safaei MR, Afrand M, Yarmand H, Zulkifli N (2019) Assessment of thermal conductivity enhancement of nano-antifreeze containing single-walled carbon nanotubes: optimal artificial neural network and curve-fitting. Phys A Stat Mech Appl 521:138–145
36. Nasiri H, Jamalabadi MYA, Sadeghi R, Safaei MR, Nguyen TK, Shadloo MS (2019) A smoothed particle hydrodynamics approach for numerical simulation of nano-fluid flows: application to forced convection heat transfer over a horizontal cylinder. J Therm Anal Calorim 135:1733–1741
37. Safaei MR, Hajizadeh A, Afrand M, Qi C, Yarmand H, Zulkifli NW (2019) Evaluating the effect of temperature and concentration on the thermal conductivity of ZnO–TiO_2/EG hybrid nanofluid using artificial neural network and curve fitting on experimental data. Phys A 519:209–216
38. Bahiraei M, Salmi HK, Safaei MR (2019) Effect of employing a new biological nanofluid containing functionalized graphene nanoplatelets on thermal and hydraulic characteristics of a spiral heat exchanger. Energy Convers Manag 180:72–82
39. Haghighi SS, Goshayeshi HR, Safaei MR (2018) Natural convection heat transfer enhancement in new designs of plate-fin based heat sinks. Int J Heat Mass Transf 125:640–647
40. Malvandi A, Safaei MR, Kaffash MH, Gahji DD (2015) MHD mixed convection in a vertical annulus filled with Al_2O_3-water nanofluid considering nanoparticle migration. J Magn Magn Mater 382:296–306
41. Nazari S, Ellahi R, Sarafraz MM, Safaei MR, Asgari A, Akbari OA (2020) Numerical study on mixed convection of a non-Newtonian nanofluid with porous media in a two lid-driven square cavity. J Therm Anal Calorim 140:1121–1145
42. Ranjbarzadeh R, Moradikazerouni A, Bakhtiari R, Asadi A, Afrand M (2019) An experimental study on stability and thermal conductivity of water/silica nanofluid: eco-friendly production of nanoparticles. J Clean Prod 206:1089–1100
43. Ranjbarzadeh R, Isfahani AM, Afrand M, Karimipour A, Hojaji M (2017) An experimental study on heat transfer and pressure drop of water/graphene oxide nanofluid in a copper tube under air cross-flow: applicable as a heat exchanger. Appl Therm Eng 125:69–79
44. Ranjbarzadeh R, Karimipour A, Afrand M, Isfahani AHM, Shirneshan A (2017) Empirical analysis of heat transfer and friction factor of water/graphene oxide nanofluid flow in turbulent regime through an isothermal pipe. Appl Therm Eng 126:538–547
45. Al-Rashed AA, Ranjbarzadeh R, Aghakhani S, Soltanimehr M, Afrand M, Nguyen TK (2019) Entropy generation of boehmite alumina nanofluid flow through a minichannel heat exchanger considering nanoparticle shape effect. Phys A 521:724–736
46. Ranjbarzadeh R, Akhgar A, Musivand S, Afrand M (2018) Effects of graphene oxide-silicon oxide hybrid nanomaterials on rheological behavior of water at various time durations and temperatures: synthesis, preparation and stability. Powder Technol 335:375–387
47. Berchet AB, Beaudoin A, Huberson SH (2020) Adaptive particle method based on moments for simulating the mass transport in natural flows. Comput Particle Mech. https://doi.org/10.1007/s40571-020-00350-5
48. Morikawa D, Senadheera H, Asai M (2020) Explicit incompressible smoothed particle hydrodynamics in a multi-GPU environment for large-scale simulations. Comput Particle Mech. https://doi.org/10.1007/s40571-020-00347-0
49. Imoto Y (2019) Unique solvability and stability analysis for incompressible smoothed particle hydrodynamics method. Comput Particle Mech 6(2):297–309
50. Imoto Y, Tsuzuki S, Nishiura D (2019) Convergence study and optimal weight functions of an explicit particle method for the incompressible Navier-Stokes equations. Comput Particle Mech 6(4):671–694
51. Su YC, Jiang S, Gan Y, Chen Z, Lu JM (2019) Investigation of the mechanical responses of copper nanowires based on molecular dynamics and coarse-grained molecular dynamics. Comput Particle Mech 6(2):177–190
52. Mayo SL, Olafson BD, Goddard WA (1990) DREIDING: a generic force field for molecular simulations. J Phys Chem 94(26):8897–8909
53. Lennard-Jones JE (1924) On the determination of molecular fields. Proc R Soc Lond A 106(738):463–477. https://doi.org/10.1098/rspa.1924.0082

54. Toukan K, Rahman A (1985) Molecular-dynamics study of atomic motions in water. Phys Rev B 31(5):2643–2648
55. Berendsen HJC, Grigera JR, Straatsma TP (1987) The missing term in effective pair potentials. J Phys Chem 91(24):6269–6271
56. Daw MS, Baskes M (1984) Embedded-atom method: derivation and application to impurities, surfaces, and other defects in metals. Phys Rev B Am Phys Soc 29(12):6443–6453
57. Rapaport DC (2004) The art of molecular dynamics simulation, 2nd edn. Cambridge University Press, Cambridge. ISBN 0-521-82568-7
58. Nosé S (1984) A unified formulation of the constant temperature molecular-dynamics methods. J Chem Phys 81(1):511–519
59. Hoover WG (1985) Canonical dynamics: equilibrium phase-space distributions. Phys Rev A 31(3):1695–1697